Received 7 October 2024; Accepted 5 November 2024
https://doi.org/10.48612/letters/2024-4-425-431
https://elibrary.ru/nrqmai

Structure, mechanical properties and strengthening mechanisms of rapidly quenched Al-based ribbons consolidated by high pressure torsion processing

E. A. Sviridova†[1,2], V. N. Varyukhin[1], S. V. Vasiliev[1,2], V. M. Tkachenko[1], V. I. Tkatch[1]

†ksvir@list.ru

[1]Galkin Donetsk Institute for Physics and Engineering, Donetsk 283048, Russia
[2]Donbas National Academy of Civil Engineering and Architecture, Makeyevka 286123, Russia

Abstract: The influence of high-pressure-torsion (HPT) processing on the structure and hardness of laminated disks consolidated from rapidly solidified ribbons of $Al_{86}Ni_9Gd_5$ and $Al_{95.8}Mn_{3.8}Fe_{0.4}$ alloys with amorphous and crystalline structures, respectively, as well as from their combination was studied using X-ray diffraction (XRD) analysis, scanning electron microscopy and microhardness measurements. The effect of the HPT deformation by unconstrained and constrained schemes on the changes of concentration of supersaturated Al-based solid solution in the as-prepared $Al_{95.8}Mn_{3.8}Fe_{0.4}$ ribbon was found. The experimentally established increase in hardness of disks consolidated from crystalline ribbons as a function of the level of deformation was quantitatively analyzed within the additive model. The contributions of grain boundary, dislocation and solid solution strengthening mechanisms were determined using the values of sizes of coherently scattering domains, microstrains and solid solution concentration found from the XRD data. The changes in the hardness of disks consolidated from $Al_{86}Ni_9Gd_5$ amorphous ribbons due to the formation of a nanocomposite structure were measured. An increase in the hardness of disks consolidated from amorphous and crystalline ribbons above the hardness value that harder disks with a nanocomposite structure was established and a possible reason of this effect caused by additional microstrains in the crystalline material due to mixing, was discussed.

Keywords: rapid solidification, high-pressure torsion, Al-based alloy, consolidation, structure, microhardness, strengthening mechanisms

Acknowledgements: *The authors are grateful to V. V. Burkhovetskii for providing the SEM images and N. V. Chernyavskaya for performing the microhardness measurements.*

1. Introduction

Metallic alloys with metastable structures play an important role in materials science from a technical point of view as well as for basic research due to the enhanced level of their physical properties. There are several techniques for achieving metastable structural states; among them the most widely used are melt quenching (rapid solidification of melts at cooling rates 10^4–10^6 K/s) and severe plastic deformation (SPD). Application of both these techniques for metallic alloys results in the grain size refinement, extending of solid solubility and the formation of metastable intermetallic and even amorphous phases [1, 2]. The majority of these structural changes lead to essential improvement of mechanical properties (ahead of all strength) therefore rapidly solidified (RS) alloys have a great potential for practical applications.

Aluminium alloys due to their low density were extensively used in applications where high specific strengths are important such as the aerospace and automotive industry. However, to produce aluminum alloys with attractive mechanical properties, high critical cooling rates of above 10^4 K/s are typically required. For this reason, the rapidly solidified products are obtained in ribbon, flakes or powder forms and it is the major obstacle that dramatically limits applications. The attempts to consolidate these products using conventional hot extrusion or pressing showed that full consolidation requires relatively high temperatures (≥673 K) [2] at which the metastable structures and the improved mechanical properties could not be retained. On the other hand, the techniques of severe plastic deformation (SPD) [3,4] which provide very large strains at relatively low temperatures are promising for consolidation of rapidly quenched materials with nonequilibrium structures.

In fact, consolidation of amorphous $Al_{86}Gd_6Ni_6Co_2$ melt-spun ribbons by twist extrusion resulted in obtaining fully dense billets with dimensions of 14 mm × 23 mm × 40 mm at temperatures ≥513 K [5]. The billet consolidated at 513 K had partially crystallized nanocomposite structure (Al nanocrystals with a size 13 ±1 nm embedded in amorphous matrix) with high microhardness (5.5 GPa). However, the $Al_{86}Gd_6Ni_6Co_2$ glass as well as a number of Al-based glasses lose their ductility at temperatures below 500 K [6] indicating that consolidation temperature for these alloys must be lower.

This problem may be solved by using the high pressure torsion (HPT) deformation procedure in which materials constrained between two anvils are subjected to SPD by

torsional straining. As has been shown, this procedure allows achieving consolidation of gas atomized $Al_{90}Fe_5Nd_5$ powders [7] and amorphous $Al_{86}Ni_9Gd_5$ ribbons [8] into bulk nanostructured disks with a nanocomposite structure at room temperature.

It should be noted that HPT straining was originally invented for producing bulk ultrafine-grained (nanostructured) materials [3]. However, later besides the mentioned consolidation of rapidly solidified materials, HPT was used to enhance the strength materials without losing their ductility [9] to develop various layered materials composites [8,10–13] as well as to produce phase transformations. These include the formation and decomposition of supersaturated solid solutions [14,15], amorphization crystalline alloys [16], and crystallization of amorphous phases [17]. The majority of these transformations result in obtaining materials with enhanced mechanical properties similar to those produced by rapid solidification. Therefore, it can be expected that the combined impact of two extreme techniques, namely, quenching from liquid state and severe plastic deformation results in a subsequent improvement in mechanical properties.

In fact, as was shown in [14] rapid solidification of the Al-1.5 wt.% Zr alloy results in enhancement of its microhardness from 300 to 700 MPa, which was subsequently increased by the HPT processing up to 1500 MPa. The observed changes were explained by increasing solid solubility of Zr in Al from nearly zero to 0.8 wt.% in the RS sample and to 1.5 wt.% Zr after HPT as well as by refinement of microstructure. However, relative contributions of the strengthening mechanisms to hardening caused by the used treatments were not established. Such quantitative analysis of the yield stress value ($\sigma_{0.2}$) of binary Al-0.4 wt.% Zr alloy subjected to HPT treatment showed [18] that the main contribution in strengthening arose from grain boundary mechanism (about 77%), while the effects of solid solution and strain hardening are relatively small (5 and 12%, respectively).

It should be noted that the sum of these contributions calculated from the structural data for the deformed sample was in good agreement with the experimentally measured value of $\sigma_{0.2}$. However, similar calculations for annealed HPT-processed samples indicate the existence of additional strengthening mechanisms.

Recent calculations using the additive approach for the contributions of different strengthening mechanisms [18,19] confirmed the dominant role of grain boundary hardening in the microhardness of the HPT disks consolidated from foils of pure Al, but also showed an increasing contribution (from 7 to 30%) of the strain (dislocation) strengthening mechanism with increasing degree of deformation [20].

The aim of the paper is to study the effect of HPT processing on disks consolidated from rapidly solidified ribbons of Al-based alloys with crystalline ($Al_{95.8}Mn_{3.8}Fe_{0.4}$) and amorphous ($Al_{86}Ni_9Gd_5$) structures and to estimate contributions of different strengthening mechanisms. It was established earlier [8,21] that these ribbons were successfully consolidated by HPT straining and the disks produced had high strength properties. The present studies were performed using both unconstrained (the disk was formed between flat anvils with a diameter of 5 mm) and constrained (the disk was treated in a circular cavity with a diameter of 5 mm in the lower anvil) types of HPT straining.

2. Materials and methods

Ribbons with nominal compositions of $Al_{86}Ni_9Gd_5$ and $Al_{95.8}Mn_{3.8}Fe_{0.4}$ (Al-7.4Mn-0.8Fe (wt.%)) were produced by melt spinning in He atmosphere and in air, respectively. For convenience, the studied alloys with crystalline and amorphous structures will be further designated as AlMnFe and AlNiGd, respectively. The effects of HPT straining were carried out on layered consolidated samples consisted of (i) two crystalline AlMnFe ribbons (55 ± 5 μm thick), (ii) two amorphous AlNiGd ribbons (65 ± 5 μm thick) and (iii) their combination (a double-folded piece of amorphous ribbon between crystalline ribbons and spot welding of the free ends of the package together). These packages were placed between the anvils with a diameter of 5 mm and deformed by rotating through N=1, 2, 4 and 6 revolutions under an applied pressure of 2 GPa at the rate of 1 rpm by constrained type of HPT. Additionally, a set of four layered disks from AlMnFe ribbons were prepared by unconstrained HPT processing by torsion for one revolution at a pressure of 2 GPa.

The structural characterization of the as-prepared ribbons and consolidated disks was performed using X-ray diffraction (XRD) and scanning electron microscopy (SEM). XRD patterns were recorded on a DRON-3M automated standard diffractometer by the step scanning method using a wavelength of with λ_{Co} = 0.1791 nm. The structural state of rapidly solidified and deformed crystalline samples was characterized by the size of the volume-averaged coherent scattering domain (CSD), $<D>$ and the level of lattice microstrain $<\varepsilon^2>^{1/2}$ proportional to the dislocation density [22]. The values of $<D>$ and $<\varepsilon^2>^{1/2}$ were determined by full-profile fitting of diffraction maxima using the approximation method [23] applied to diffraction patterns obtained using nonchromatic radiation. The calculations described in detail in [20,21] were carried out, assuming that the Gaussian form of each reflection profile is a convolution of the profiles formed by microstrains β_S and by the dispersed sizes of coherently scattering domains (CSD) β_D. It gives:

$$\langle D \rangle = \frac{\lambda}{\beta_D \cos(\theta)} \quad (1)$$

and

$$\langle \varepsilon^2 \rangle^{1/2} = \frac{\beta_S}{\sqrt{2\pi}\tan(\theta)} \quad (2)$$

where θ is the diffraction angle.

Microhardness H_μ was measured on a standard hardness tester PMT-3 with a 136° diamond pyramid indenter. The measurements were performed under a load of 0.49 N for 10 s along the diameter of the disks approximately at a distance of 0.25 mm. In view that the XRD data characterize full surface of the discs, the values of H_μ were determined by averaging all indents as

$$\langle H_\mu \rangle_S = 2\pi \int_0^R H(r) r dr / \pi R^2 \cdot$$

Data scatter is estimated as about ±10% of the average value in each case.

The morphological features of internal structure of consolidated disks were studied on polished surfaces of fractured samples using a scanning electron microscopy (JSM-6490LV).

3. Results

The experiments showed that the scheme of HPT processing influenced both shape and structure of the consolidated disks. Four layered AlMnFe disks with diameter of 5 mm had a slightly convex shape with thickness changing from 165 to 135 μm from center to periphery which is typical for this type of deformation [8]. In contrast, the disks consolidated by a constrained version of HPT had a relatively constant thickness of about 200 μm. XRD studies showed that the unconstrained deformation resulted in the appearance of weak lines in the consolidated disk pattern in addition to the peaks corresponding to fcc Al-based solid solution presented in the pattern of rapidly solidified ribbon (Fig. 1). Besides, as can be seen, the positions of the solid solution peaks shifted to smaller angles in pattern *b*, indicating an increase in the lattice parameter.

The analysis of the XRD data showed that the lattice constants of fcc Al in the initial rapidly solidified ribbon (0.40322 ± 0.00003 nm) and in the disk consolidated using the unconstrained scheme (0.40425 ± 0.00007 nm) were lower than that of pure Al (0.40496 nm) [24]. In view that atomic radii of Mn and Fe (0.130 and 0.127 nm, respectively) are lower than that of Al (0.143 nm) it indicated that the unconstrained consolidation resulted in decreasing concentration in solid solution. It is known [1], the results of rapid solidification in extending solute solubility and in part, in the binary Al-Mn system, the equilibrium limit of 1.4 wt.% [25] was increased up to 10 wt.% [26]. As it was established in [26], the lattice constant of Al(Mn) solid solution linearly decreased with a concentration of Mn with a slope of -3.3×10^{-4} nm/wt.%. If we neglect the effect of Fe (due to its low content), these results indicate that the unconstrained HPT treatment leads to decreasing concentration in the supersaturated solid solution from 5.27 wt.% in the initial ribbon to 2.15 wt.%. In turn, a decrease in the concentration of Mn in solid solution results in the formation of intermetallic compound (the most probably Al_4Mn [26]).

In contrast, the peaks of Al-based solid solution of in the disk consolidated using the constrained HPT processing shift to high angles (Fig. 1). The lattice constant in this disk is lower (0.40302 ± 0.00004 nm) than that in the initial rapidly solidified ribbon and this value corresponds to the concentration of 5.88 wt.% Mn. This indicates that the deformation using this scheme results in an increase ni supersaturation of the solid solution.

In spite of the structural differences, the average microhardness of the disks consolidated using different schemes of HPT after 1 revolution was the same, namely 2.04 GPa, appreciably higher than H_μ of as-prepared ribbon (1.18 GPa). The increase in the deformation strain led to a subsequent enhancement of microhardness up to 2.91 GPa after 6 revolutions (Fig. 2). According to the relationship between the yield strength and the hardness of metals and alloys $H/\sigma_{0.2}=3$ [27] this value of H_μ corresponds to $\sigma_{0.2}$ about 1 GPa, which is a very high value for crystalline Al-based alloys.

The XRD studies showed that diffraction patterns of the disks consolidated using the constrained scheme were similar to that of rapidly solidified ribbon (Fig. 1a) and contained only peaks of Al-based solid solution. The detailed analysis of the patterns showed that the deformation resulted in changes of solid solubility from 5.9 wt.% after 1 and 2 revolutions to about 5.1 wt.% after 4 and 6 revolutions, while the values of CSD and microstrains were in the ranges of 32 – 48 nm and $(2.6-3.1)\times10^{-3}$, respectively, and had not clear dependence on the level of deformation.

As it was recently established, the layered HPT consolidated disks consisted of crystalline and amorphous rapidly solidified ribbons had essentially high hardness [8,28]. In the present study the two-layered disks consisted of amorphous AlNiGd ribbons and four-lavered (a double-folded piece of amorphous

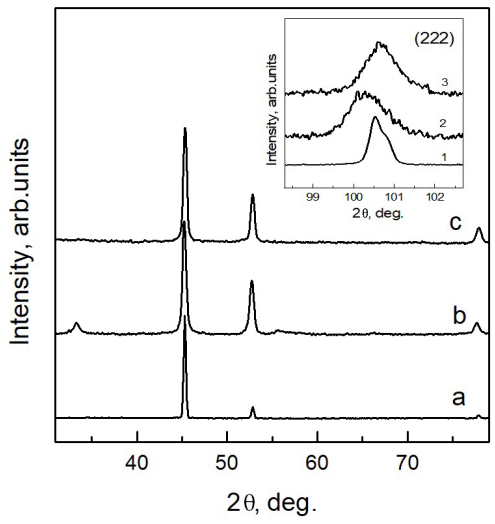

Fig. 1. XRD patterns of AlMnFe samples: rapidly solidified ribbon, (5.3 wt.% Mn) (a), disks consolidated using the unconstrained scheme, (2.2 wt.% Mn) (b), disks consolidated using the constrained scheme (5.9 wt.% Mn) (c).

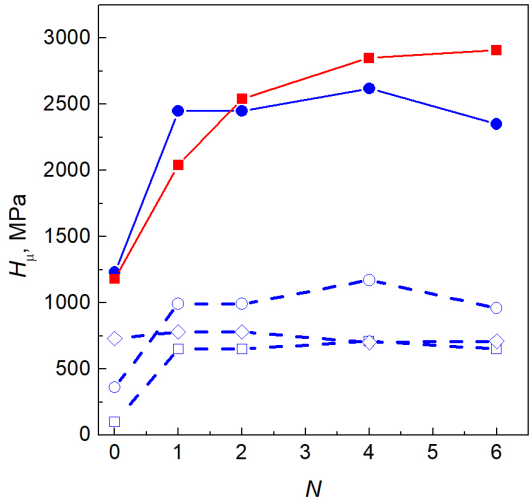

Fig. 2. (Color online) Average hardness of the two-layered disks consolidated from rapidly solidified AlMnFe ribbons at an applied pressure of 2 GPa as a function of number of revolutions: ■ — experiment, calculated summary curve (●) and contributions from grain boundary hardening (○), strain hardening (□) and solid solution hardening (◇) mechanisms.

ribbon between crystalline ribbons) were consolidated using the constrained HPT processing at 2 GPa up to 6 revolusions. The measurements of microhardness of the consolidated disks showed that with increasing strain, the values of H_μ of amorphous ribbons increased from 2.7 GPa with saturation up to 4.25 ± 0.25 GPa (Fig. 3).

The observed behavior of microhardness of consolidated amorphous ribbons as a function of the level of deformation is typical [5,7,8] and as shown in Fig. 4 it is caused by the deformation-induced crystallization (formation of the nanocomposite structure consisted of Al nanocrystals embedded in the residual amorphous matrix). The disks consolidated from crystalline AlMnFe ribbons after all applied deformations retain the structure of supersaturated solid solution (Fig. 4) therefore the effect of its hardening is caused by changes of a thin structure as will be considered below.

At the same time, the hardness of hybrid disks being average between those of amorphous and crystalline discs after from 1 to 3 revolutions then (after 4 and 6 revolutions) became higher than H_μ of the disks consisted of amorphous ribbons and approached 5.2 GPa (Fig. 3). In view that the phase composition and the structure of surface disks consolidated from crystalline ribbons and amorphous ribbon inside crystalline are similar (Fig. 4), the possible reason of enhanced hardness of hybrid disks is caused by differences of internal microstructure.

The SEM studies showed that the degree of deformation influenced the macroscopic structure (Fig. 5). As can be seen in the laminated structure consisted of separated layers of different materials, which was formed at initial stages of deformation (Fig. 5 a) the vortex-like mixing began at higher deformation levels (Fig. 5 b). The similar structural features were observed in the three-layered disk consolidated by HPT from the crystalline rapidly solidified AlCrMoTiZrV ribbon placed between two amorphous AlNiGd ribbons [8] in which the areas with the mixed structure had very high (above 5 GPa) microhardness.

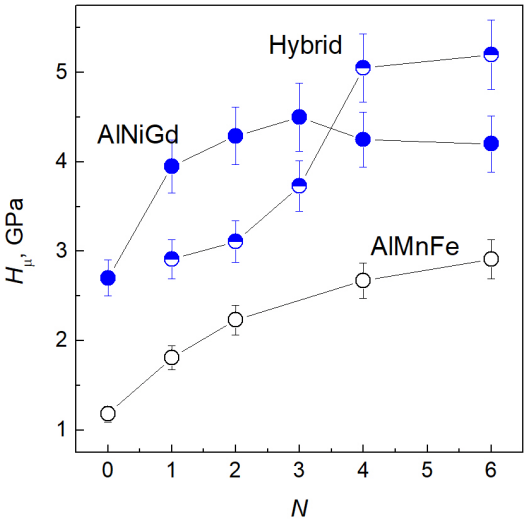

Fig. 3. (Color online) Average microhardness of the disks consisted of crystalline AlMnFe ribbons (open symbols), amorphous AlNiGd ribbons (dark symbols) and their combination (combined symbols) consolidated at applied pressure of 2 GPa as a function of number of turns.

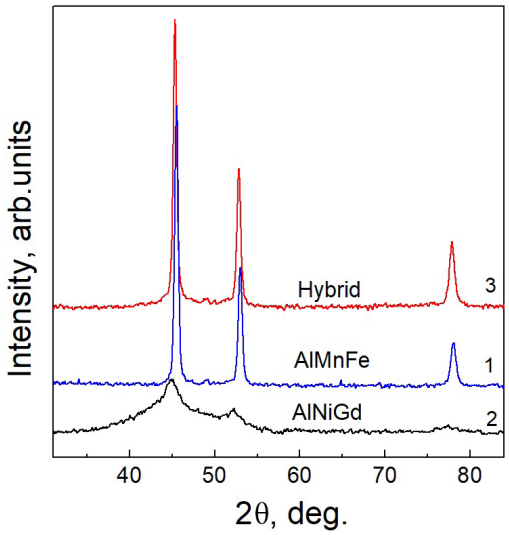

Fig. 4. (Color online) XRD patterns of the surface of the disks consolidated under the pressure of 2 GPa from crystalline AlMnFe ribbons (1), amorphous AlNiGd ribbons (2) and their combination (3) for $N = 4$.

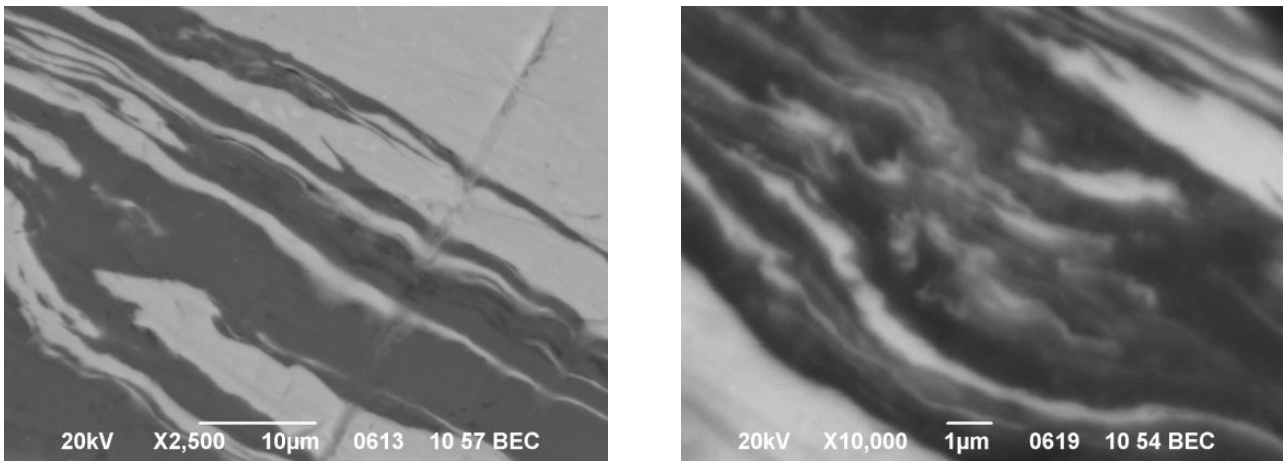

a b

Fig. 5. Microstructure of polished cross-section of four-layered disk consisted of amorphous AlNiGd ribbons (light) placed between the crystalline AlMnFe ribbons (dark) consolidated at 2 GP for 2 (a) and 4 (b) turns.

4. Discussion

It should be noted here that similar result (the values of hardness of composite disk superior to those of constituents) was observed in the disks consolidated by HPT from two amorphous ribbons $Fe_{53.3}Ni_{26.5}B_{20.2}$ and $Co_{28.2}Fe_{38.9}Cr_{15.4}Si_{0.3}B_{17.2}$ [29]. It was assumed that the possible reason of additional hardening was the formation of intermetallic phase particles at boundaries of ribbons. However, this assumption is not valid for the combination of $Al_{86}Ni_9Gd_5$ and $Al_{95.1}Cr_{2.5}Mo_{1.4}Ti_{0.4}Zr_{0.3}V_{0.3}$ ribbons due to a low content of alloying elements in the crystalline alloy. On the other hand, most probably, the additional hardening is caused by vortex-like microscopic mixing observed at certain levels of deformation shown in Fig. 5b. This mixing which arises during the HPT processing of layered disks composed of materials with different strength characteristics may result in the formation of additional stresses in a softer material [30,31].

As it was shown above, the rapidly solidified AlMnFe ribbon had relatively high microhardness (1.2 GPa), which was subsequently increased by HPT straining up to 2.91 GPa (Fig. 2). In order to clarify mechanisms responsible for the observed hardening, the structural characteristics (size of CSD, level of microstrains and concentration of Al-based solid solution) of the ribbon and disks were used to calculate the contributions of different strengthening mechanisms into the value of yield stress $\sigma_{0.2}$ within the additive approach [19]. In view that according to the XRD data all AlMnFe samples had a single phase structure of the Al-based solid solution, the contributions of only grain boundary σ_{gb}, dislocation (microstrain) σ_{disl} and solid solution σ_{ss} hardening mechanisms were considered, i.e.

$$\sigma_{0.2}^{th} = \sigma_0 + \sigma_{gb} + \sigma_{disl} + \sigma_{ss} \quad (3)$$

where σ_0 is the Peierls-Nabarro stress was taken to be 10 MPa as in [19].

The grain-boundary contribution was calculated using the Hall–Petch relationship [32]: $\sigma_{gb} = KD^{-1/2}$, where K is the Hall–Petch coefficient taken to be 0.07 MPa·m$^{1/2}$ [33]. The contribution of dislocation strengthening was estimated by the Taylor formula [34]

$$\sigma_{dis} = M\alpha GbL_{dis}^{1/2} \quad (4)$$

where $M = 3.06$ is the Taylor factor, $\alpha = 0.33$ is the parameter of interdislocation interaction [35], G is the shear modulus of Al equal to 26 GPa, b is the Burgers vector value (0.286 nm) and L_d is the dislocation density [22]:

$$L_d = \frac{2\sqrt{3}\langle \varepsilon^2 \rangle^{1/2}}{\langle D \rangle b} \quad (5)$$

The contribution from solid solution hardening was estimated as [36]:

$$\sigma_{ss} = \sum k_i \left(C_i^{ss}\right)^{2/3} \quad (6)$$

where the coefficient $k_{Mn} = 80.0$ MPa/wt.%$^{2/3}$ was taken from [37] and C_{Mn}^{ss} is concentration of Al(Mn) solid solution.

The values of the yield stress were calculated from Eqs. (3) – (6) using the structural data (D, $<\varepsilon^2>^{1/2}$ and C_{Mn}^{ss}) determined from XRD studies and then were recalculated into H_μ as $3\sigma_{0.2}$ [27]. The calculations showed that hardness of the initial rapidly solidified ribbon was presumably determined by solid solution (60%) and grain boundary (29%) strengthening mechanisms and the calculated value of hardness (1230 MPa) was in a good agreement with that experimentally measured (1180 MPa). The HPT processing led to a twofold increase in microhardness to 2040 – 2910 MPa presumably due to the growth of contributions of grain boundary (up to 1–1.17 GPa) and dislocation (0.65 – 0.7 GPa) strengthening mechanisms (Fig. 2). They are in turn caused by a decrease in CSD sizes from 350 to 32 – 48 nm and an increase in the density of dislocation from 2.5×10^{13} to about $(8-9)\times10^{14}$ m^{-2}. It should be noted that a similar effect of the increase in the density of dislocation from 0.4×10^{13} to 2.3×10^{13} m^{-2} caused by HPT treatment was observed for the aged Al-1.47Cu-0.34Zr alloy [19].

The data presented in Fig. 2 show that the model calculations of the contributions of grain boundary, dislocation and solid solution strengthening mechanisms are in reasonable agreement with the experimental data. The lower calculated value of H_μ after 6 revolutions may be caused by a lower concentration of solid solution from 5.9 to 5.03 wt.% and which results in the formation of particles of the intermetallic phase (precipitation hardening). More detailed structural data are needed to account for this strengthening mechanism.

It was established that the HPT deformation may result both in the formation [14] and in the decomposition [15] of supersaturated solid solutions. These effects are related to the degree of metastability which is created by certain conditions of processing [15]. The experiments described above (Fig. 1) showed that the HPT deformation using the unconstrained scheme led to lowering of the Al-based solid solution concentration from 5.3 to 2.2 wt.% Mn, while using the constrained type of HPT resulted in an increase in solid solubility of Mn up to 5.9. This may indicate that enhancement of the degree of metastability is caused by the presence of back-pressure in the constrained scheme. Additional experiments are required to confirm this assumption.

5. Conclusions

The studies of the influence of (HPT) processing on the structure and hardness of laminated disks consolidated from rapidly solidified ribbons of $Al_{86}Ni_9Gd_5$ and $Al_{95.8}Mn_{3.8}Fe_{0.4}$ alloys with amorphous and crystalline structures showed:

1. It was found that HPT treatment of AlMnFe ribbon using the unconstrained scheme resulted in partial decomposition of the supersaturated Al-based solid solution (lowering Mn concentration from 5.3 to 2.2 wt.%) while deformation with using the constrained scheme led to an increase in supersaturation up to 5.9 wt.%.

2. The increase in the level deformation (number of revolutions) led to an increase in microhardness of two-layered AlMnFe disks from 1180 to 2910 MPa after 6 revolutions.

3. It was established that with using the XRD structural data, the observed changes of microhardness of AlMnFe ribbon and disks may be reasonably quantitatively approximated within the additive model involving grain boundary, dislocation and solid solution strengthening mechanisms.

4. The calculations showed that the microhardness of the initial rapidly solidified AlMnFe ribbon was presumably determined by solid solution (60%) and grain boundary (29%) strengthening mechanisms, while the deformation resulted in an increase in the contribution from the dislocation mechanism (from 10 to 26 – 28%) due to the increase in the density of dislocations (from 2.5×10^{13} to about $(8-9)\times10^{14}$ m^{-2}).

5. It was established that at certain deformation degree, the microhardness of the hybrid disks (composed of amorphous and crystalline ribbons) became higher than the microhardness of that harder disks consisted of amorphous ribbons. The possible reason for the superior hardness of the hybrid disks is the formation of additional stresses in crystalline ribbon during vortex-like mixing of the materials with different hardness.

References

1. H. Jones, Spalt cooling and metastable phases, Rep. Prog. Phys. 36 (1973) 1425 –1497.
2. A. Inoue, Amorphous, nanoquasicrystalline and nanocrystalline alloys in Al-based systems, Progr. Mater. Sci. 43 (1998) 365 – 520.
3. R.Z. Valiev, R.K. Islamgaliev, I.V. Alexandrov, Bulk nanostructured materials from severe plastic deformation, Progr. Mater. Sci. 45 (2000) 103 –189.
4. R.Z. Valiev, B. Straumal, T.G. Langdon, Using severe plastic deformation to produce nanostructured materials with superior properties, Annu. Rev. Mater. Res. 52 (2022) 357 – 382.
5. V.N. Varyukhin, V.I. Tkatch, V.V. Maslov, Y.Y. Beygelzimer, S.G. Synkov, V.K. Nosenko, S.G. Rassolov, A.S. Synkov, V.I. Krysov, V.A. Mashira, Consolidation of amorphous $Al_{86}Ni_6Co_2Gd_6$ melt-spun ribbons by twist extrusion, Mater. Sci. Forum 503 – 504 (2006) 699 – 704.
6. E.A. Sviridova, V.V. Maksimov, S.G. Rassolov, V.K. Nosenko, V.I. Tkatch, Influence of the chemical composition of Al-based amorphous alloys on thermally induced embrittlement, Phys. Solid State 56 (2014) 1355 –1362.
7. A.R. Yavari, W.J. Botta Fihlo, C.A. D. Rodrigues, C. Cardoso, R.Z. Valiev, Nanostructured bulk $Al_{90}Fe_5Nd_5$ prepared by cold consolidation of gas atomized powder using severe plastic deformation, Scripta Mater. 46 (2002) 711 – 716.
8. S.V. Vasiliev, A.I. Limanovskii, V.M. Tkachenko, T.V. Tsvetkov, K.A. Svyrydova, V.V. Burkhovetskii, V.N. Sayapin, S.V. Terekhov, V.I. Tkatch, Fabrication of consolidated layered samples by high-pressure torsion processing of rapidly solidified Al-based ribbons with amorphous and crystalline structures, Mater. Today Commun. 24 (2020) 101080.
9. Y.B. Wang, D.D. Qu, X.H. Wang, Y. Cao, X.Z. Liao, M. Kawasaki, S.P. Ringer, Z.W. Shan, T.G. Langdon, J. Shen, Introducing a strain-hardening capability to improve the ductility of bulk metallic glasses via severe plastic deformation, Acta Mater. 60 (2012) 253 – 260.
10. T. Mo, Z. Chen, Z. Zhou, J. Liu, W. He, Q. Liu, Enhancing of mechanical properties of rolled 1100/7075 Al alloys laminated metal composite by thermomechanical treatments, Mater. Sci. Eng. A 800 (2021) 140313.
11. G. Korznikova, R. Kabirov, K. Nazarov, R. Khisamov, R. Shayakhmetov, E. Korznikova, G. Khalikova, R. Mulyukov, Influence of constrained high-pressure torsion on microstructure and mechanical properties of an aluminum-based metal matrix composite, JOM 72 (2020) 2898 – 2911.
12. P. Bazarnik, A. Bartkowska, B. Romelczyk-Baishya, B. Adamczyk-Cieslak, J. Dai, M. Lewandowska, T.G. Langdon, Superior strength of tri-layered Al-Cu-Al nano-composites processed by high-pressure torsio, J. Alloys Compds. 846 (2020) 156380.
13. G.F. Korznikova, E.A. Korznikova, G.R. Khalikova, K.S. Nazarov, R.Kh. Khisamov, S.N. Sergeev, R.U. Shayakhmetov, R.R. Mulyukov, Al based layered in situ metal-matrix composites fabricated by constrained high pressure torsion, Letters on Materials 11 (2021) 533 – 543.
14. I.G. Brodova, D.V. Bashlykov, A.B. Manukhin, V.V. Stolyarov, E.P. Soshnikova, Formation of nanostructure in rapidly solidified Al-Zr alloy by severe plastic deformation, Scr. Mater. 44 (2001) 1761–1764.
15. B.B. Straumal, B. Baretzky, A.A. Mazilkin, F. Phillipp, O.A. Kogtenkova, M.N. Volkov, R.Z. Valiev, Formation of nanograined structure and decomposition of supersaturated solid solution during high pressure torsion of Al-Zn and Al-Mg alloys, Acta Mater. 52 (2004) 4469 – 4478.
16. B.B. Straumal, A.R. Kilmametov, A.A. Mazilkin, S.G. Protasova, K.I. Kolesnikova, P.B. Straumal, B. Baretzky, Amorphization of Nd-Fe-B alloy under the action of high-pressure torsion, Mater. Lett. 145 (2015) 63 – 66.
17. A.M. Glezer, S.V. Dobatkin, M.R. Plotnikova, A.V. Shalimova, Severe plastic deformation of amorphous alloys, Mater. Sci. Forum 584 – 586 (2008) 227 – 230.
18. T.S. Orlova, T.A. Latynina, A.M. Mavlyutov, M.Y. Murashkin, R.Z. Valiev, Effect of annealing on microstructure, strength and electrical conductivity of the pre-aged and HPT-processed Al-0.4Zr alloy, J. Alloys Compd. 791 (2019) 947 – 951.
19. T.S. Orlova, D.I. Sadykov, M.Yu. Murashkin, V.U. Kazykhanov, N.A. Enikeev, Peculiarities of strengthening of Al-Cu-Zr alloy structured by severe plastic deformation, Phys. Solid State 63 (2021) 1744 –1756.
20. E.A. Sviridova, S.V. Vasiliev, A.I. Limanovskii, V.N. Varyukhin, V.I. Tkatch, Mechanisms of strengthening aluminum foils consolidated by the high-pressure-torsion technique, J. Surf. Investig. 18 (2024) 623 – 629.
21. K.A. Svyrydova, T.V. Tsvetkov, V.M. Tkachenko, A.I. Limanovskii, V.N. Sayapin, S.V. Vasiliev, V.I. Tkatch, Structure and mechanical properties of rapidly cooled Al-based alloys consolidated by high pressure torsion technique, Transactions of the Kola science centre. Chemistry and materials 12 (2021) 219 – 225. (in Russian)
22. G.K. Williamson, R.E. Smallman, Dislocation densities

in some annealed and cold-worked metals from measurements on the X-ray Debye-Scherrer spectrum, Philos. Mag. 1 (1956) 34 – 46.
23. S. S. Gorelik, Yu. A. Skakov, L. N. Rastorguev, X-Ray and Electron-Optical Analysis, MISIS, Moscow, 2002, 357 p. (in Russian)
24. G. V. Samsonov (Ed), Properties of the elements. Handbook. Part 1, Metallurgy, Moscow, 1976, 600 p. (in Russian)
25. N. P. Lyakishev (Ed), Diagrams of the state of double metal systems. Handbook, Mechanical engineering, Moscow, 1996, 992 p. (in Russian)
26. A. A. Yakunin, I. I. Osipov, V. I. Tkatch, A. B. Lysenko, The effect of melt quenching and heat treatment on the structure and properties of aluminum-manganese alloys, Phys. Metals Metallogr. 43 (1977) 140 –144. (in Russian)
27. P. Zhang, S. X. Li, Z. F. Zhang, General relationship between strength and hardness, Mater. Sci. Eng. A 529 (2011) 62 – 73.
28. S. V. Vasiliev, E. A. Sviridova, A. I. Limanovskii, V. M. Tkachenko, T. V. Tsvetkov, V. V. Burkovetskii, V. N. Varyukhin, V. I. Tkatch, Structure and mechanical properties of layered composites, consolidated by high pressure torsion of amorphous and crystalline Al alloys, Phys. Solid State 65 (2023) 2132 – 2137. DOI: 10.61011/PSS.2023.12.57685.223 Webpage
29. I. E. Permyakova, A. M. Glezer, A. I. Kovalev, O. V. Vahrushev, Three-stage evolution of the structure and the effect of nonadditive hardening of layered composites from amorphous alloys under high-pressure torsion, JETP Letters 113 (2021) 468 – 474. (in Russian)
30. R. Kulagin, Y. Beygelzimer, Yu. Ivanisenko, A. Mazilkin, B. Straumal, H. Hahn, Instabilities of interfaces between dissimilar metals induced by high pressure torsion, Mater. Lett. 222 (2018) 172 –175.
31. Y. Beygelzimer, A. Filippov, Y. Estrin, 'Turbulent' shear flow of solids under high-pressure torsion, Philos. Mag 103 (2023) 1017–1028.
32. E. O. Hall, The deformation and aging of mild steel: III Discussion of results, Proc. Phys. Soc. B 64 (1951) 747 – 753.
33. D. B. Witkin, E. J. Lavernia, Synthesis and mechanical behavior of nanostructured materials via cryomilling, Progr. Mater. Sci. 51 (2006) 1 – 60.
34. N. Hansen, X. Huang, Microstructure and flow stress of polycrystals and single crystals, Acta Mater. 46 (1998) 1827 –1836.
35. F. R. N. Nabarro, Z. S. Basinski, D. B. Holt, The plasticity of pure single crystals, Adv. Phys. 13 (1964) 193 – 323.
36. O. R. Myhr, Ø. Grong, S. J. Andersen, Modelling of the age hardening behaviour of Al-Mg-Si alloy, Acta Mater. 49 (2001) 65 – 75.
37. O. R. Myhr, Ø. Grong, C. Schafter, An extended age-hardening model for Al-Mg-Si alloys incorporating the room-temperature storage and cold deformation process stages, Metall. Mater. Trans. A 46 (2015) 6018 – 6039.